ACS OMEGA

Article

Cite This: ACS Omega XXXX, XXX, XXX−XXX

http://pubs.acs.org/journal/acsodf

Fabrication of Concentric Carbon Nanotube Rings and Their Application on Regulating Cell Growth

Hu Li,[†] Luming Zhao,[‡,§] Weibo Zhu,[⊥] Xuecheng Qu,[‡,§] Chan Wang,[‡,§] Ruping Liu,[⊥] Yubo Fan,*[,†,∥] and Zhou Li*[,‡,§,#]

[†]Beijing Advanced Innovation Centre for Biomedical Engineering, Key Laboratory for Biomechanics and Mechanobiology of Chinese Education Ministry, School of Biological Science and Medical Engineering, Beihang University, Beijing 100083, China

[‡]CAS Center for Excellence in Nanoscience, Beijing Key Laboratory of Micro−Nano Energy and Sensor, Beijing Institute of Nanoenergy and Nanosystems, Chinese Academy of Sciences, Beijing 100083, China

[§]College of Nanoscience and Technology, University of Chinese Academy of Sciences, Beijing 100049, China

[∥]National Research Center for Rehabilitation Technical Aids, Beijing 100176, China

[⊥]School of Printing and Packaging Engineering, Beijing Institute of Graphic Communication, Beijing 102600, China

Supporting Information

ABSTRACT: The carbon nanotube (CNT) pattern plays an important role in various electronic devices and biological fields for its superior conductivity and biocompatibility. Herein, we fabricated regularly arranged concentric multiwalled carbon nanotube (MWCNT) rings in a Petri dish by evaporation-driven self-assembly technology. By adjusting the dispersion ratio, heating temperature, and solution volume, various MWCNT rings with different shapes and morphologies were obtained. The variation law of ring radius, formation range, and ring numbers was processed with statistical analysis. With fine adjustment of parameters, the control of desired MWCNT rings can be achieved for further scientific researches. By culturing L929 cells with these rings, oriented cell growth along the rings was achieved, which is of significance for cell regulation, tissue repairing, and related biological applications.

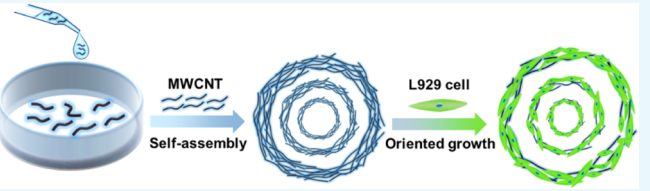

1. INTRODUCTION

Carbon nanotubes (CNTs) have attracted substantial attention because of their exceptional electrical, mechanical, and biological performance.[1−4] In many scientific research studies, CNTs were used as additives to enhance the mechanical property and conductivity of bioengineering scaffolds,[5−7] or used for neural signal amplification, disease treatment, and tissue engineering.[8−10] For these applications, the location and arrangement of cell growth on CNTs are crucial to achieve the desired experiment effect. In view of this goal, many remarkable works were carried out on regular CNT patterns, including parallel CNT lines,[11,12] square CNTs,[13] individual CNTs,[14] and so on. These CNT patterns were usually prepared by a template, photo-lithography, or chemical vapor deposition technique.[11−13,15,16] Aside from these precision technologies, evaporation-driven self-assembly provided another alternative technique for the fabrication of regular nanomaterial patterns.[17−21]

When the multiwalled carbon nanotube (MWCNT) dispersion solution was confined in a circular vessel device, MWCNT will self-assemble into concentric rings after water evaporation.[21] With the solvent evaporation, liquid convection occurred from inner space to edge to replenish the lost liquid. With the increase in concentration, parts of solutes dissolved out from the solvent, and then the solutes were carried to the triple-phase contact line of vapor−liquid−solid by convection and deposited on the substrate. With the pinning and receding of the contact line, regular patterns formed.[17−22] Besides the shape of geometric construction, there are also many other factors affecting the formation of MWCNT rings. In the previous work,[21] the self-assembly mechanism of MWCNT rings on various substrates with different Hamaker constants were studied. Besides the mechanism, the regulation of other ring properties also has significance on specific application scenarios (e.g., biological effect), including the ring shape, ring position, ring number, and ring-formation range.

In this work, we studied the self-assembly of MWCNT rings in a Petri dish. The influence of reagent ratio, heating temperature, and solution volume is studied in detail. The properties of ring formation were analyzed by statistical means. After culturing L929 cells with MWCNT rings together, the cells achieved selective growth along the ring direction. By this study, researchers can obtain expected MWCNT rings with specific parameters, which can be used for their designed experiments. The as-fabricated MWCNT rings provided feasible induction cues and scaffolds for regulating cell growth,

Received: August 1, 2019
Accepted: September 9, 2019

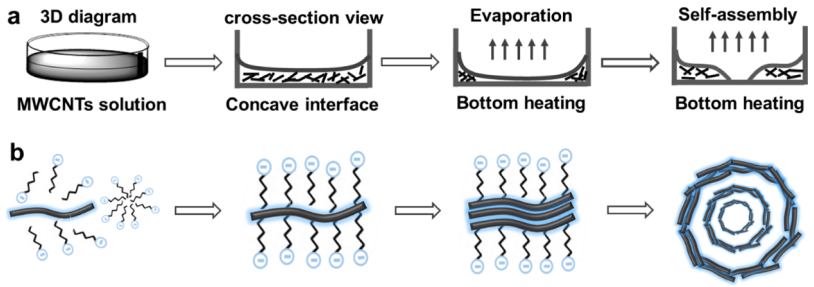

Figure 1. (a) Self-assembly diagram of concentric MWCNT rings in a Petri dish. (b) Dispersion diagram of MWCNTs in water. The ball-and-stick model represents the SDBS molecule. The stick and ball represent the hydrophobic and hydrophilic ends of SDBS, respectively.

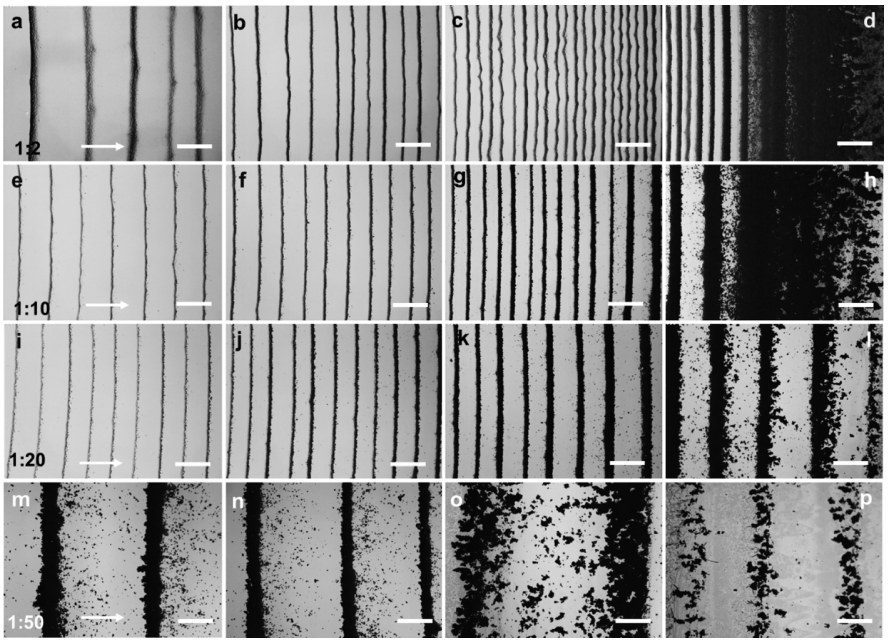

Figure 2. MWCNTs self-assembly with different MWCNT/SDBS ratios. (a–d) 1:2; (e–h) 1:10; (i–l) 1:20; (m–p) 1:50. Scale bar: 200 μm. The arrows represent the receding direction of the triple-phase contact line and the direction of formation of MWCNT rings from the center to outer edge of the Petri dish.

which has significance for cell regulation, tissue repairing, and related biological field.

2. RESULTS AND DISCUSSION

2.1. Fabrication Diagram of Concentric MWCNT Rings. As shown in Figure 1a, the self-assembly process of concentric MWCNT rings is illustrated by a three-dimensional diagram and its cross-sectional view. At the initial stage, MWCNTs dispersion was injected in a Petri dish, and a concave interface was formed due to the combined action of gravity and capillary force. Then the dish was subjected to bottom heating. With water evaporation, MWCNTs were continually carried to the triple-phase contact line of vapor–liquid–solid by convection flow. With the triple-phase contact line receding and pinning, MWCNTs self-assembled into concentric rings on the bottom of the Petri dish.

As a commonly used surfactant, sodium dodecyl benzene sulfonate (SDBS) showed outstanding ability in dispersing CNTs in water among various surfactants.[23] It has decent binding affinity to CNT sidewalls, which can be ascribed to the benzene ring forming $\pi-\pi$ interactions on CNT sidewalls.[24] Such $\pi-\pi$ interactions enable CNTs achieve high dispersion in water.[25] As shown in Figure 1b, MWCNTs and SDBS were added to water. After ultrasonication treatment, SDBS is dissolved in water, the hydrophilic ends head for water, and hydrophobic ends absorb on the MWCNT surface. With water evaporation, the concentration of MWCNTs dispersion increases gradually, and some MWCNTs aggregate into a bundle. Under the action of liquid convection, the bundles were deposited along the circular triple-phase contact line and self-assembled into concentric rings.[21] Many factors will affect the self-assembly process and lead to various MWCNT patterns, such as the ratio of MWCNT/SDBS, heating temperature, and liquid volume. In the following parts, these three parameters were studied in detail.

2.2. MWCNTs Self-Assembly with Different MWCNT/SDBS Ratios. In the preparation of MWCNTs dispersion solution, SDBS was selected as the dispersing agent to improve the hydrophobic property of MWCNTs in water. The SDBS content will affect the dispersion state of MWCNTs, and then influences the self-assembly pattern. The heating temperature and solution volume were 80 °C and 1 mL, respectively. As shown in Figures 2 and S1, various ratios of MWCNT/SDBS were studied from 1:2 to 1:50. The morphologies of MWCNT rings were recorded along the radial direction of the Petri dish from the center to outer edge. The white arrows represent the

DOI: 10.1021/acsomega.9b02449
ACS Omega XXXX, XXX, XXX–XXX

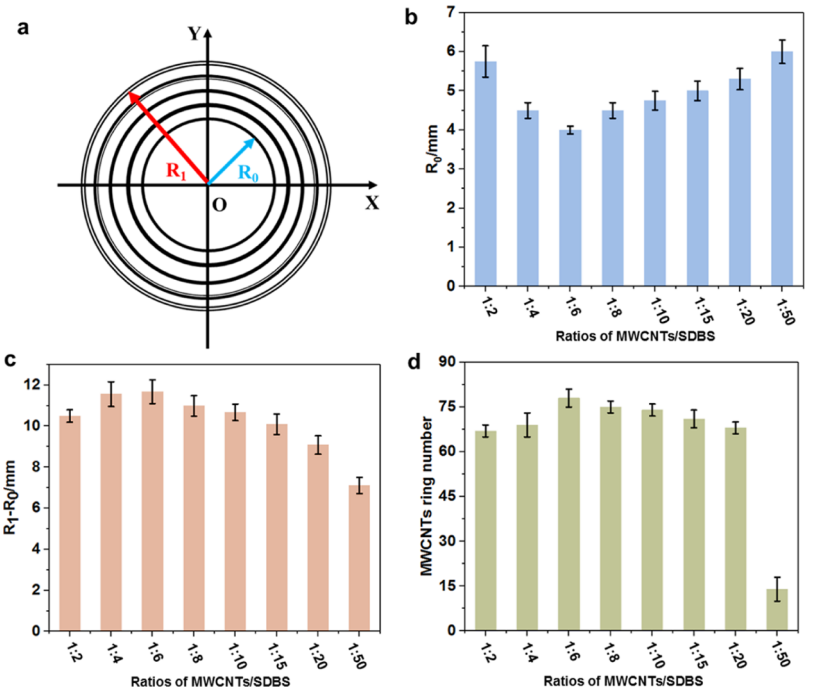

Figure 3. (a) Statistical approach of ring radius. (b) Variation trend of R_0 with different ratios of MWCNT/SDBS. (c) Variation trend of $R_1 - R_0$ with different ratios of MWCNT/SDBS. (d) Variation trend of the MWCNT ring number with different ratios of MWCNT/SDBS.

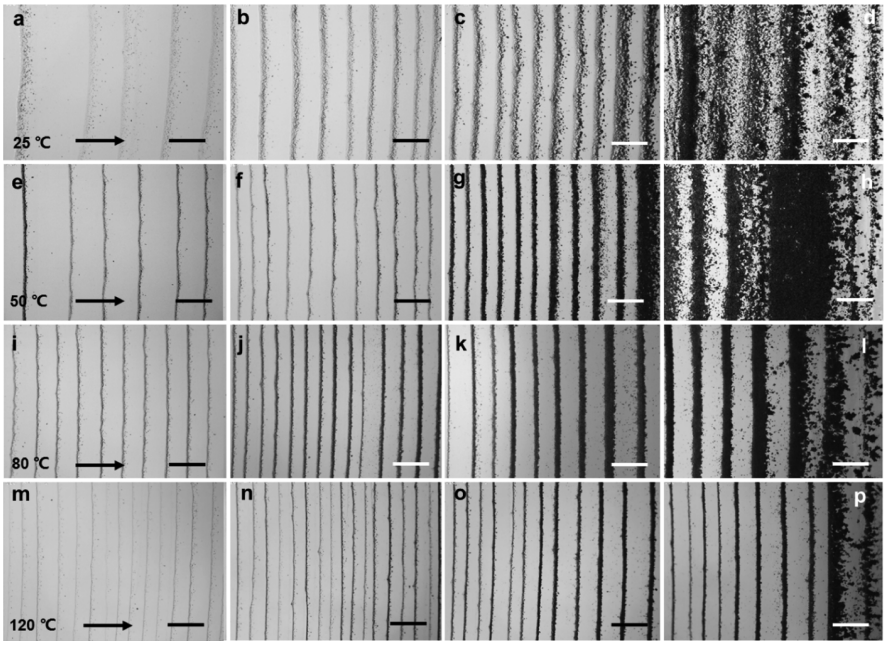

Figure 4. MWCNTs self-assembly at different heating temperatures. (a–d) 25; (e–h) 50; (i–l) 80; (m–p) 120 °C. Scale bar: 200 μm. The arrows represent the receding direction of the triple-phase contact line and the direction of formation of MWCNT rings from the center to outer edge of the Petri dish.

receding direction of the triple-phase contact line during water evaporation, and they also show the direction of formation of MWCNT rings from the center to outer edge (e.g., 1:2 from Figure 2a–d).

When the ratio is low (1:2), MWCNT rings have some wavy sites along the rings (Figure 2a,c). These wavy sites also appear at other ratios, 1:4 and 1:6 (Figure S1). With the ratio increase, the wavy sites disappeared from 1:10 to 1:50. The edges of MWCNT rings become smoother. The widths of the rings become larger from Figure 2b,f,j to 2n and from 2c,g,k to 2o. At the outer edges, the continuous MWCNT films gradually change into individual rings from Figure 2d,h,l to 2p. When the ratio is too high (1:50), inner particles in MWCNT rings at the outer edge were discrete and discontinuous (Figure 2p). Additionally, the size of MWCNT bundles or particles also become larger because the higher SDBS content can make more MWCNTs disperse in water. When equal amounts of water were evaporated gradually, more MWCNTs at a higher ratio can aggregate together into lager bundles or particles than those at a lower ratio.

DOI: 10.1021/acsomega.9b02449
ACS Omega XXXX, XXX, XXX−XXX

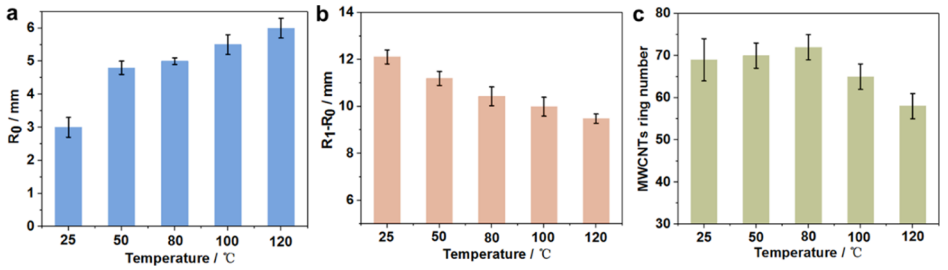

Figure 5. (a) Variation trend of R_0 at different heating temperatures. (b) Variation trend of $R_1 - R_0$ at different heating temperatures. (c) Variation trend of ring number at different heating temperatures.

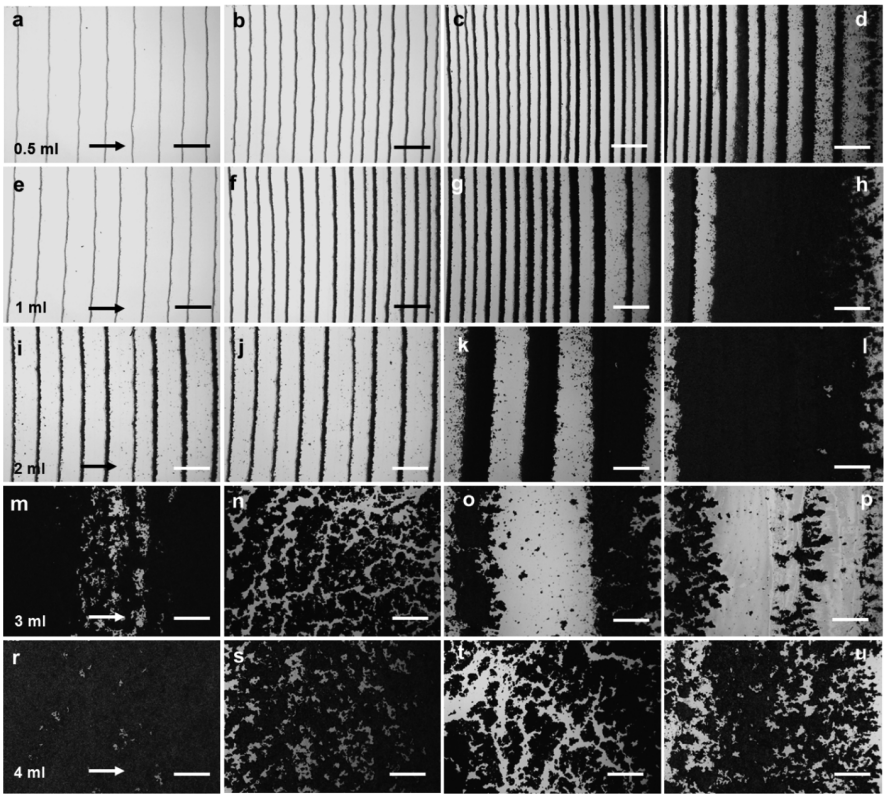

Figure 6. MWCNTs self-assembly with different volumes. (a–d) 0.5; (e–h) 1; (i–l) 2; (m–p) 3; (q–t) 4 mL. Scale bar: 200 μm. The arrows represent the receding direction of the triple-phase contact line and the direction of formation of MWCNT rings from the center to outer edge of the Petri dish.

The ring number and radii of the first ring and last ring were counted. Figure 3a shows the statistical approach of R_0 and R_1 along the radial direction. R_0 represents the radius of the first MWCNT ring at the center position of the Petri dish. R_1 represents the radius of the last MWCNT ring at the outer edge of the Petri dish. $R_1 - R_0$ represents the formation range of MWCNT rings. As shown in Figure 3b, R_0 decreases first, and then increases with the ratios. When the ratio is 1:6, R_0 is the shortest, about 4 mm. From Figure 3c, $R_1 - R_0$ reaches a maximum range of about 11.7 mm. Meanwhile, the number of self-assembled MWCNT rings is also the largest, about 78 (Figure 3d). According to these results, we can fabricate the most number of MWCNT rings, the widest ring rang at 1:6, and the least number of MWCNT rings at 1:50.

2.3. MWCNTs Self-Assembly with Different Heating Temperatures. Based on the results in shown in Figure 2, a ratio of 1:10 and volume of 1 mL were selected for the following temperature study. The heating temperature will affect the evaporation rate of water, which further influences the receding rate of the triple-phase contact line and the aggregation of MWCNT bundles. Therefore, the heating temperature will also bring change to ring formation. The rings are recorded from the center to the outer edge of the Petri dish along the radial direction.

As shown in Figure 4a, the first few rings include a small quantity of MWCNTs, the ring spaces vary from 200 to 400 μm. The quantity of MWCNTs increases along the radial direction from Figure 4a–d. At the outer edge of the Petri dish (Figure 4d), MWCNT rings connect with each other, like a film. This can be attributed to the slow receding rate of the triple-phase contact line, which leads to the continuous deposition of MWCNTs at a low temperature. With the temperature increasing from 25 to 120 °C, the receding rate of the triple-phase contact line becomes faster, and the ring spaces narrow down, which vary from 160 to 240 μm in Figure 4e, 100 to 140 μm in Figure 4i, and 80 to 100 μm in Figure 4m. This trend also appeared in other positions along the vertical direction in Figure 4, such as 4b to 4n, 4c to 4o, and 4d

DOI: 10.1021/acsomega.9b02449
ACS Omega XXXX, XXX, XXX−XXX

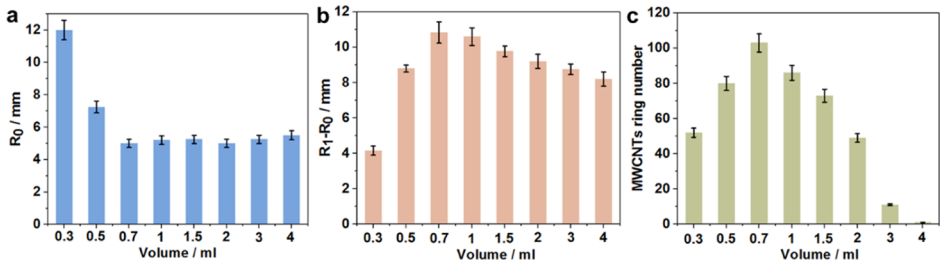

Figure 7. (a) Variation trend of R_0 with different volumes. (b) Variation trend of $R_1 - R_0$ with different volumes. (c) Variation trend of the ring number with different volumes.

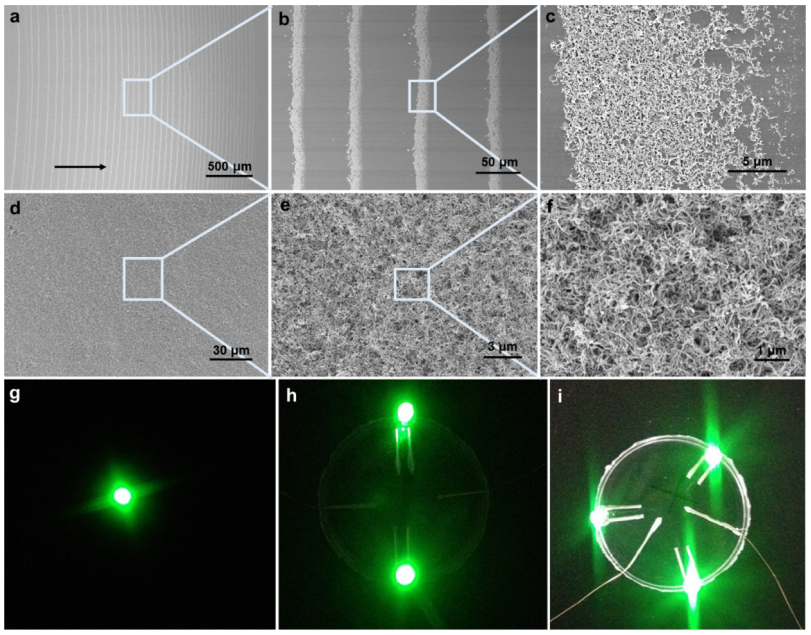

Figure 8. (a–c) Morphology characterization of MWCNT rings. (d–f) Morphology characterization of continuous MWCNT film. (g–i) Conductivity demonstration of MWCNT rings by lighting up green LEDs. The arrow represents the receding direction of the triple-phase contact line and the direction of formation of MWCNT rings from the center to outer edge of the Petri dish.

to 4p. At the outer edge of the Petri dish, the continuous MWCNT film transforms into individual rings from 4d to 4h and 4l to 4p. This can be attributed to the higher heating temperature, which makes the triple-phase contact line recede easier and faster than at low temperature. Then MWCNTs are deposited as individual rings along the circular receding triple-phase contact line.

The variation trends of R_0, $R_1 - R_0$, and the ring numbers with heating temperatures are recorded in Figure 5. R_0 increases with the increase of heating temperature (Figure 5a). This is because of the fact that the higher heating temperature leads to more evaporation within the same time and induces a bigger surface tension for the receding of the triple-phase contact line. Therefore, the first ring at high heating temperature has a larger radius than at low heating temperature. The ring formation range decreases with the increase of heating temperature (Figure 5b). Meanwhile, the ring number increases first and then decreases with the heating temperature (Figure 5c). The ring numbers from 25 to 80 °C are close, and then the numbers fall rapidly from 80 to 120 °C. This may be caused by the fast thermal movement of MWCNT bundles at higher temperature, and plenty of MWCNTs are deposited on few rings during a short self-assembly time.

2.4. MWCNTs Self-Assembly with Different Volumes.

In this part, a ratio of 1:10 and a heating temperature of 80 °C are chosen for the study of volume effect on MWCNTs self-assembly. The morphologies of MWCNT rings are recorded along the radial direction from the center to outer edge of the Petri dish. The ring images at 0.3, 0.7, and 1.5 mL are shown in Figure S2. The average space between the two adjacent rings shows a decreasing trend along the radial direction with a volume of 0.5, 1, and 2 mL (Figure 6a–d,e–h,i–l). The widths of the single rings become wider along the radial direction at every volume. With volume increase, the width changes of the rings are the most obvious along the vertical direction in Figure 6 (Figure 6a,e,i, b,f,j, c,g,k, d,h,l). The widths of rings become wider with the increasing volume. When the volume is 3 mL, the rings nearly disappeared. At the center position, continuous MWCNT films formed (Figure 6m,n). At the outer edge of the Petri dish, few scatter-like rings are formed (Figure 6o,p). When the volume is larger than 3 mL (e.g., 4 mL), the rings completely disappeared. A circular MWCNT film is formed.

As shown in Figure 7a, the radius of the first ring (R_0) decreases with the volume, and then changes a little bit only after 0.7 mL. This indicates that a volume of 0.7 mL can generate rings at the earliest time. Meanwhile, a volume of 0.7 mL also has the widest ring range as shown in Figure 7b.

DOI: 10.1021/acsomega.9b02449
ACS Omega XXXX, XXX, XXX−XXX

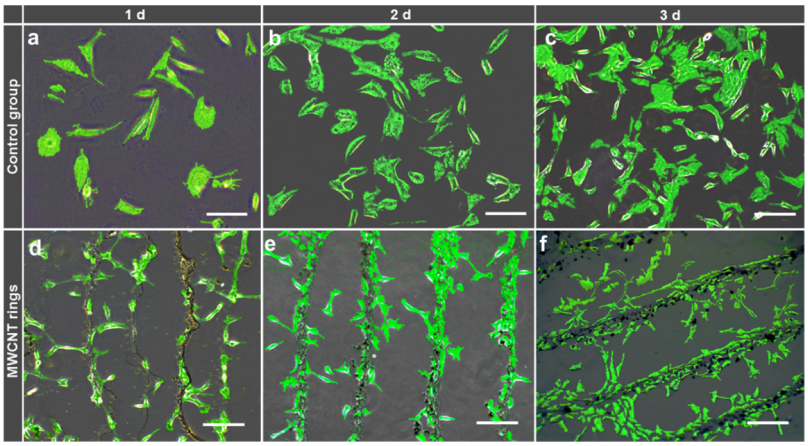

Figure 9. L929 cell culture without MWCNT rings as a control group for (a) 1, (b) 2, and (c) 3 days. L929 cell culture with MWCNT rings for (d) 1, (e) 2, and (f) 3 days. All the cells were processed by pseudocolor technology. Scale bar: 200 μm.

Additionally, most ring numbers also appear at this volume (Figure 7c). According to these statistical results shown in Figure 7 and morphologies in shown in Figure 6, if the ring number is expected, a volume of 0.7 mL will be an optimized parameter. If a continuous MWCNT film is expected, a volume of more than 4 mL will be an optimized parameter.

2.5. Morphology Characterization by Scanning Electron Microscope and Conductivity Demonstration. To study the micromorphology of MWCNTs, two types of representative self-assembled MWCNTs were characterized by scanning electron microscope (SEM), including the rings and continuous film. The rings and film were prepared using 1 and 4 mL of solution, respectively, at 80 °C. The ratio of MWCNT/SDBS is 1:10. Before the SEM characterization, the nonconducting SDBS was washed and removed by treatment with deionized water and nitric acid. Figure 8a shows the regular ring formation under a large field of view, about 43 rings. From the enlarged views (Figure 8b,c), it is shown that the ring edges are smooth, and MWCNTs deposited together into a continuous network, which ensured its conductivity when used as a circuit. As shown in Figure 8d, when the MWCNT solution is excess (i.e., 4 mL), the rings transformed into a continuous film. The film surface has a porous structure (Figure 8e), and MWCNTs intertwined with each other (Figure 8f). To demonstrate the conductivity of MWCNT rings, the cylindrical wall of the Petri dish was dismantled, and green light-emitting diodes (LEDs) were fixed on the rings using silver paste with three modes, including one LED at free position (Figure 8g), two LEDs at opposite positions (Figure 8h), and three LEDs at average positions (Figure 8i). After applying a voltage (5 V) on the rings, the green LED can be lighted up immediately, indicating its good conductivity as a conductive circuit.

2.6. MWCNT Rings for Regulating Cell Growth. CNT-based devices have wide applications in cell engineering, and the oriented cell growth on CNT pattern has key function in these scenarios.[8−10,26−28] The oriented growth and proliferation of L929 cells play an important role in wound repair. The L929 cells can synthesize and secrete plenty of collagen fiber and matrix components, which promote the formation of granulation tissue and create favorable conditions for the coverage of epidermal cells.[29−31] In this experiment, the L929 cells were selected for studying its oriented growth and proliferation on MWCNT rings.

To make it convenient to observe the cell morphologies, MWCNT rings with low density were used for L929 cell culture. The rings were prepared at 25 °C with 1 mL of MWCNT dispersion solution. The ratio of MWCNT and SDBS is 1:10. As shown in Figure 9a−c, L929 cells were seeded and cultured in a Petri dish without MWCNT rings as a control group. On the first day, the cells are sparse with normal cellular morphologies. The cell density rapidly increases with culture time in 2 days (Figure 9b). When the culture reached 3 days, some cells grew into clusters (Figure 9c). All the cells grow randomly in the Petri dish.

Compared with the control group, the cells cultured with MWCNTs showed regular growth along the rings. Some cells showed the growth tendency along scattered rings with a low cell density. The other cells grew between two adjacent rings (Figure 9d). With the increasing culture time, the cell density also increased, and the number of cells on rings clearly increased. A few number of cells grow between rings. And some of their pseudopods were connected with the ring edge (Figure 9e). With the proliferation of cells, the cell density on rings increased, some cells grew into clusters on rings, most of the cells oriented along the ring direction, and a few number of cells migrated to the space, like a bridge, between two adjacent rings (Figure 9f). The selective adhesion and growth of cells on MWCNT rings can be attributed to the strong affinity between MWCNTs and extracellular matrix proteins.[12] These results indicate that the as-fabricated MWCNT rings can provide an effective induction factor for regulating cell growth. The oriented growth and proliferation of L929 cells proved the feasibility and potential of using as-fabricated MWCNT rings as a scaffold and inducement for wound healing, tissue repairing, and related biological applications.

3. CONCLUSIONS

In summary, regular concentric MWCNT rings were fabricated successfully in Petri dishes. By changing the ratio of MWCNT/SDBS, heating temperature, and solution volume, the self-assembly of MWCNTs can transform from rings to films gradually, and the number, radius, and formation range of MWCNT rings can be tuned. The fine adjustment of parameters provided a deep understanding of MWCNT self-assembly, and it is of significant reference value for controlling the self-assembly of other nanomaterials in the Petri dish system. The rings can be used as a circular circuit for other

DOI: 10.1021/acsomega.9b02449
ACS Omega XXXX, XXX, XXX−XXX

electronic devices due to their conductive property. When culturing L929 cells with MWCNT rings, the cells showed oriented growth and proliferation along the ring direction, which proved the feasibility and potential of using MWCNT rings as a scaffold and inducement for cell engineering, such as oriented cell growth, tissue repairing, and related biological applications.

4. EXPERIMENTAL SECTION

4.1. Preparation of MWCNT Dispersion Solution. The MWCNT powder was purchased from Shenzhen Nanotech Port Co. Ltd and used without further purification. The fabrication method of MWCNTs was chemical vapor deposition. SDBS was purchased from Sigma. A mixture of MWCNT and SDBS with different ratios were put in water (30 mL) and sonicated at 100 W for 2 h. The weight of MWCNTs was fixed at 1.5 mg. Then the dispersion solution was centrifuged at 5000 rpm for 20 min. The supernatant was used for the self-assembly of MWCNT rings.

4.2. Fabrication of MWCNT Rings. When studying the ratios, the solution volume and heating temperature were fixed at 1 mL and 80 °C, respectively. When studying the heating temperatures, the ratio of MWCNT/SDBS and solution volume were fixed at 1:10 and 1 mL, respectively. When studying the solution volume, the ratio of MWCNT/SDBS and heating temperature were fixed at 1:10 and 80 °C, respectively. The Petri dish was purchased from Beijing Hualide Technology Co., Ltd, the inner diameter was 35 mm, and the constituent material is polystyrene.

4.3. Characterization of MWCNT Rings and L929 Cells. The morphologies of the MWCNT rings were recorded by using an optical metallographic microscope (DM 2500, Leica) with a HC PLAN s objective (10 × 25 Br. M). The micromorphology of MWCNT rings and films was characterized by SEM (SU 8020). The heating process was carried out on a heating plate. Before the cell culture and SEM characterization, the SDBS on MWCNT rings was dissolved many times by immersion in deionized water and nitric acid.[32−34] To make it convenient to observe the cell morphologies, MWCNT rings with low density were used for L929 cell culture. The rings were prepared at 25 °C with 1 mL of MWCNT dispersion solution. The ratio of MWCNT and SDBS is 1:10. The L929 cells were seeded in the Petri dish and cultured in Dulbecco's modified Eagle medium containing 10% fetal bovine serum, 100 U mL^{-1} penicillin, and 100 μg mL^{-1} streptomycin. The L929 cells were incubated in a cell incubator with a humidity atmosphere containing 5% CO_2 at 37 °C for 1, 2, and 3 days, respectively.[35,36]

■ ASSOCIATED CONTENT

Supporting Information

The Supporting Information is available free of charge on the ACS Publications website at DOI: 10.1021/acsomega.9b02449.

Optical images of MWCNT rings with different MWCNT/SDBS ratios and different solution volumes (PDF)

■ AUTHOR INFORMATION

Corresponding Authors

*E-mail: yubofan@buaa.edu.cn (Y.F.).
*E-mail: zli@binn.cas.cn (Z.L.).

ORCID

Chan Wang: 0000-0001-6002-5304
Zhou Li: 0000-0002-9952-7296

Present Address

#Beijing Institute of Nanoenergy and Nanosystems, Chinese Academy of Sciences, Beijing 100083, China; Yubo Fan, Beijing Advanced Innovation Centre for Biomedical Engineering, Beihang University, Beijing 100083, China.

Notes

The authors declare no competing financial interest.

■ ACKNOWLEDGMENTS

The authors thank the support of National Key R&D Project from Minister of Science and Technology, China (2016YFA0202703), the National Natural Science Foundation of China (nos. 61875015, 31571006, 81601629, 21801019, 61971049, and 11421202), the Beijing Natural Science Foundation (2182091), the Beijing Municipal Science and Technology Commission (Z181100004418004), the Research and Development Program of BIGC (Ec201808), and the National Youth Talent Support Program.

■ REFERENCES

(1) Avouris, P.; Chen, Z.; Perebeinos, V. Carbon-based electronics. *Nat. Nanotechnol.* **2007**, *2*, 605−615.
(2) Meng, Y.; Xu, X.-B.; Li, H.; Wang, Y.; Ding, E.-X.; Zhang, Z.-C.; Geng, H.-Z. Optimisation of carbon nanotube ink for large-area transparent conducting films fabricated by controllable rod-coating method. *Carbon* **2014**, *70*, 103−110.
(3) Yuan, X.-S.; Guo, Z.-Y.; Geng, H.-Z.; Rhen, D. S.; Wang, L.; Yuan, X.-T.; Li, J. Enhanced performance of conductive polysulfone/MWCNT/PANI ultrafiltration membrane in an online fouling monitoring application. *J. Membr. Sci.* **2019**, *575*, 160−169.
(4) Tian, Y.; Zhang, X.; Geng, H.-Z.; Yang, H.-J.; Li, C.; Da, S.-X.; Lu, X.; Wang, J.; Jia, S.-L. Carbon nanotube/polyurethane films with high transparency, low sheet resistance and strong adhesion for antistatic application. *RSC Adv.* **2017**, *7*, 53018−53024.
(5) Pok, S.; Vitale, F.; Eichmann, S. L.; Benavides, O. M.; Pasquali, M.; Jacot, J. G. Biocompatible carbon nanotube-chitosan scaffold matching the electrical conductivity of the heart. *ACS Nano* **2014**, *8*, 9822.
(6) Shin, S. R.; Farzad, R.; Tamayol, A.; Manoharan, V.; Mostafalu, P.; Zhang, Y. S.; Akbari, M.; Jung, S. M.; Kim, D.; Comotto, M.; Annabi, N.; Al-Hazmi, F. E.; Dokmeci, M. R.; Khademhosseini, A. A bioactive carbon nanotube-based ink for printing 2D and 3D flexible electronics. *Adv. Mater.* **2016**, *28*, 3280.
(7) Ren, J.; Xu, Q.; Chen, X.; Li, W.; Guo, K.; Zhao, Y.; Wang, Q.; Zhang, Z.; Peng, H.; Li, Y.-G. Superaligned carbon nanotubes guide oriented cell growth and promote electrophysiological homogeneity for synthetic cardiac tissues. *Adv. Mater.* **2017**, *29*, 1702713.
(8) Cellot, G.; Cilia, E.; Cipollone, S.; Rancic, V.; Sucapane, A.; Giordani, S.; Gambazzi, L.; Markram, H.; Grandolfo, M.; Scaini, D.; Gelain, F.; Casalis, L.; Prato, M.; Giugliano, M.; Ballerini, L. Carbon nanotubes might improve neuronal performance by favouring electrical shortcuts. *Nat. Nanotechnol.* **2009**, *4*, 126−133.
(9) Kam, N. W. S.; O'Connell, M.; Wisdom, J. A.; Dai, H. Carbon nanotubes as multifunctional biological transporters and near-infrared agents for selective cancer cell destruction. *Proc. Natl. Acad. Sci. U.S.A.* **2005**, *102*, 11600−11605.
(10) Harrison, B. S.; Atala, A. Carbon nanotube applications for tissue engineering. *Biomaterials* **2007**, *28*, 344−353.
(11) Park, S. Y.; Park, S. Y.; Namgung, S.; Kim, B.; Im, J.; Kim, J. Y.; Sun, K.; Lee, K. B.; Nam, J.-M.; Park, Y.; Hong, S. Carbon nanotube monolayer patterns for directed growth of mesenchymal stem cells. *Adv. Mater.* **2007**, *19*, 2530−2534.

DOI: 10.1021/acsomega.9b02449
ACS Omega XXXX, XXX, XXX−XXX

(12) Namgung, S.; Kim, T.; Baik, K. Y.; Lee, M.; Nam, J.-M.; Hong, S. Fibronectin-carbon-nanotube hybrid nanostructures for controlled cell growth. *Small* **2011**, *7*, 56−61.
(13) Baik, K. Y.; Park, S. Y.; Heo, K.; Lee, K.-B.; Hong, S. Carbon nanotube monolayer cues for osteogenesis of mesenchymal stem cells. *Small* **2011**, *7*, 741−745.
(14) Namgung, S.; Baik, K. Y.; Park, J.; Hong, S. Controlling the growth and differentiation of human mesenchymal stem cells by the arrangement of individual carbon nanotubes. *ACS Nano* **2011**, *5*, 7383−7390.
(15) Zhang, X.; Prasad, S.; Niyogi, S.; Morgan, A.; Ozkan, M.; Ozkan, C. Guided neurite growth on patterned carbon nanotubes. *Sens. Actuators, B* **2005**, *106*, 843−850.
(16) Hong, S. W.; Jeong, W.; Ko, H.; Kessler, M. R.; Tsukruk, V. V.; Lin, Z. Directed self-assembly of gradient concentric carbon nanotube rings. *Adv. Funct. Mater.* **2008**, *18*, 2114−2122.
(17) Han, W.; Lin, Z. Learning from "coffee rings": Ordered structures enabled by controlled evaporative self-Assembly. *Angew. Chem., Int. Ed.* **2012**, *51*, 1534−1546.
(18) Kang, S. H.; Shin, Y. C.; Hwang, E. Y.; Lee, J. H.; Kim, C.-S.; Lin, Z.; Hur, S. H.; Han, D.-W.; Hong, S. W. Engineered "coffee-rings" of reduced graphene oxide as ultrathin contact guidance to enable patterning of living cells. *Mater. Horiz.* **2019**, *6*, 1066−1079.
(19) Li, H.; Hain, T. C.; Muzha, A.; Schöppler, F.; Hertel, T. Dynamical contact line pinning and zipping during carbon nanotube coffee stain formation. *ACS Nano* **2014**, *8*, 6417−6424.
(20) Li, B.; Han, W.; Byun, M.; Zhu, L.; Zou, Q.; Lin, Z. Macroscopic highly aligned DNA nanowires created by controlled evaporative self-assembly. *ACS Nano* **2013**, *7*, 4326−4333.
(21) Li, H.; Ouyang, H.; Yu, M.; Wu, N.; Wang, X.; Jiang, W.; Liu, Z.; Tian, J.; Jin, Y.; Feng, H.; Fan, Y.; Li, Z. Thermo-driven evaporation self-assembly and dynamic analysis of homocentric carbon nanotube rings. *Small* **2017**, *13*, 1603642.
(22) Deegan, R. D.; Bakajin, O.; Dupont, T. F.; Huber, G.; Nagel, S. R.; Witten, T. A. Capillary flow as the cause of ring stains from dried liquid drops. *Nature* **1997**, *389*, 827.
(23) Moore, V. C.; Strano, M. S.; Haroz, E. H.; Hauge, R. H.; Smalley, R. E.; Schmidt, J.; Talmon, Y. Individually suspended single-walled carbon nanotubes in various surfactants. *Nano Lett.* **2003**, *3*, 1379−1382.
(24) Li, H.; Zhou, L.; Wu, T. Sodium dodecyl benzene sulfonate for single-walled carbon nanotubes separation in gel chromatography. *Diam. Relat. Mater.* **2018**, *88*, 189−192.
(25) McDonald, T. J.; Engtrakul, C.; Jones, M.; Rumbles, G.; Heben, M. J. Kinetics of PL quenching during single-walled carbon nanotube rebundling and diameter-dependent surfactant interactions. *J. Phys. Chem. B* **2006**, *110*, 25339−25346.
(26) Wang, J.; Wang, H.; He, T.; He, B.; Thakor, N. V.; Lee, C. Investigation of low-current direct stimulation for rehabilitation treatment related to muscle function loss using self-powered TENG system. *Adv. Sci.* **2019**, *6*, 1900149.
(27) Wang, H.; Wang, J.; He, T.; Li, Z.; Lee, C. Direct muscle stimulation using diode-amplified triboelectric nanogenerators (TENGs). *Nano Energy* **2019**, *63*, 103844.
(28) Lee, S.; Wang, H.; Xian Peh, W. Y.; He, T.; Yen, S.-C.; Thakor, N. V.; Lee, C. Mechano-neuromodulation of autonomic pelvic nerve for underactive bladder: A triboelectric neurostimulator integrated with flexible neural clip interface. *Nano Energy* **2019**, *60*, 449−456.
(29) Wang, A.; Liu, Z.; Hu, M.; Wang, C.; Zhang, X.; Shi, B.; Fan, Y.; Cui, Y.; Li, Z.; Ren, K. Piezoelectric nanofibrous scaffolds as in vivo energy harvesters for modifying fibroblast alignment and proliferation in wound healing. *Nano Energy* **2018**, *43*, 63−71.
(30) Sornkamnerd, S.; Okajima, M. K.; Matsumura, K.; Kaneko, T. Surface-selective control of cell orientation on cyanobacterial liquid crystalline gels. *ACS Omega* **2018**, *3*, 6554−6559.
(31) Wu, Q.; Maire, M.; Lerouge, S.; Therriault, D.; Heuzey, M.-C. 3D printing of microstructured and stretchable chitosan hydrogel for guided cell growth. *Adv. Biosyst.* **2017**, *1*, 1700058.
(32) Li, H.; Geng, H.-Z.; Meng, Y.; Wang, Y.; Xu, X.-B.; Ding, E.-X.; Gao, J.; Chen, L.-T.; Ma, S. Fabrication and test of adhesion enhanced flexible carbon nanotube transparent conducting films. *Appl. Surf. Sci.* **2014**, *313*, 220−226.
(33) Li, H.; Wang, X.; Jiang, W.; Fu, H.; Liang, X.; Zhang, K.; Li, Z.; Zhao, C.; Feng, H.; Nie, J.; Liu, R.; Zhou, G.; Fan, Y.; Li, Z. Alkali metal chlorides based hydrogel as eco-friendly neutral electrolyte for bendable solid-state capacitor. *Adv. Mater. Interfaces* **2018**, *5*, 1701648.
(34) Geng, H.-Z.; Kim, K. K.; So, K. P.; Lee, Y. S.; Chang, Y.; Lee, Y. H. Effect of acid treatment on carbon nanotube-based flexible transparent conducting films. *J. Am. Chem. Soc.* **2007**, *129*, 7758−7759.
(35) Li, H.; Zhao, C.; Wang, X.; Meng, J.; Zou, Y.; Noreen, S.; Zhao, L.; Liu, Z.; Ouyang, H.; Tan, P.; Yu, M.; Fan, Y.; Wang, Z. L.; Li, Z. Fully bioabsorbable capacitor as an energy storage unit for implantable medical electronics. *Adv. Sci.* **2019**, *6*, 1801625.
(36) Jiang, W.; Li, H.; Liu, Z.; Li, Z.; Tian, J.; Shi, B.; Zou, Y.; Ouyang, H.; Zhao, C.; Zhao, L.; Sun, R.; Zheng, H.; Fan, Y.; Wang, Z. L.; Li, Z. Fully bioabsorbable natural-materials-based triboelectric nanogenerators. *Adv. Mater.* **2018**, *30*, 1801895.

DOI: 10.1021/acsomega.9b02449
ACS Omega XXXX, XXX, XXX−XXX